ACS APPLIED MATERIALS & INTERFACES

Research Article

www.acsami.org

Synthesis and Characterization of Novel Plasmonic Ag/AgX-CNTs (X = Cl, Br, I) Nanocomposite Photocatalysts and Synergetic Degradation of Organic Pollutant under Visible Light

Huixian Shi,[†] Jiangyao Chen,[†] Guiying Li,[†] Xin Nie,[†,⊥] Huijun Zhao,[‡] Po-Keung Wong,[§] and Taicheng An*[,†]

[†]State Key Laboratory of Organic Geochemistry and Guangdong Key Laboratory of Environmental Resources Utilization and Protection, Guangzhou Institute of Geochemistry, Chinese Academy of Sciences, Guangzhou 510640, China

[‡]Centre for Clean Environment and Energy, Griffith Scholl of Environment, Griffith University, Queensland 4222, Australia

[§]School of Life Sciences, The Chinese University of Hong Kong, Shatin, NT, Hong Kong SAR, China

[⊥]University of Chinese Academy of Sciences, Beijing 100049, China

Supporting Information

ABSTRACT: A series of novel well-defined Ag/AgX (X = Cl, Br, I) loaded carbon nanotubes (CNTs) composite photocatalysts (Ag/AgX-CNTs) were fabricated for the first time via a facile ultrasonic assistant deposition−precipitation method at the room temperature (25 ± 1 °C). X-ray diffraction, X-ray photoelectron spectroscopy, nitrogen adsorption−desorption analysis, scanning electron microscopy, and ultraviolet−visible light absorption spectra analysis were used to characterize the structure, morphology, and optical properties of the as-prepared photocatalysts. Results confirmed the existence of the direct interfacial contact between Ag/AgX nanoparticles and CNTs, and Ag/AgX-CNTs nanocomposites exhibit superior absorbance in the visible light (VL) region owing to the surface plasmon resonance (SPR) of Ag nanoparticles. The fabricated composite photocatalysts were employed to remove 2,4,6-tribromophenol (TBP) in aqueous phase. A remarkably enhanced VL photocatalytic degradation efficiency of Ag/AgX-CNTs nanocomposites was observed when compared to that of pure AgX or CNTs. The photocatalytic activity enhancement of Ag/AgX-CNTs was due to the effective electron transfer from photoexcited AgX and plasmon-excited Ag(0) nanoparticles to CNTs. This can effectively decrease the recombination of electron−hole pairs, lead to a prolonged lifetime of the photoholes that promotes the degradation efficiency.

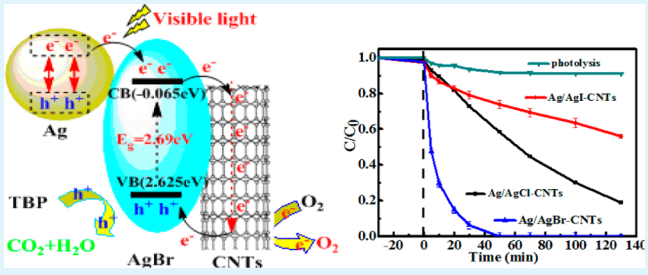

KEYWORDS: *plasmonic photocatalyst, carbon nanotube supporter, silver halides, visible light, photocatalytic activity*

INTRODUCTION

Photocatalysis technique, as a cost-effective means for solar energy utilization, hydrogen production, and environmental purification, has been focused by many researchers.[1−7] In recent years, highly efficient visible-light-driven (VLD) photocatalyst development has been recognized as an important goal in the field of photocatalysis. Generally, two major approaches have been frequently employed to fabricate VLD photocatalyst. One is to modify TiO_2-based photocatalyst to extend the light absorption spectrum from the UV to VL region by elements doping,[2] noble metal deposition,[3,8] and dye sensitization.[9] Another is to purposely fabricate new forms of VLD photocatalyst, such as Bi_5O_7I,[10] $(AgNbO_3)_{1-x}(SrTiO_3)_x$,[11] and $(Ag_{0.75}Sr_{0.25})(Nb_{0.75}Ti_{0.25})O_3$.[12] Despite the noticeable progress, these VLD photocatalysts still have some drawbacks, such as relatively low VL photocatalytic activity and poor stability, limiting their practical applications. It is therefore highly desirable to develop highly efficient VLD photocatalysts that could meet the needs for applications in environmental and energy fields.

Currently, the localized surface plasmon resonance (SPR) effect of noble-metal nanoparticles (e.g., Ag and Au) has become a research focus in the development of VLD photocatalysts.[13] The VL activity of plasmonic photocatalyst is originated from the distinctive plasmon resonance effect in VL region that has been well demonstrated for metallic Au and Ag nanoparticles.[4,14−19] Also a number of Ag/AgX (X = Cl, Br)-based materials, such as graphene sheets grafted Ag/AgCl,[1] graphene oxide (GO) enwrapped Ag/AgX (X = Cl, Br) nanocomposite,[16] Ag/AgBr@TiO_2,[18] Ag/AgCl@$H_2WO_4{\cdot}3H_2O$ composite,[4] and AgBr/WO_3[20] have recently been successfully synthesized. These composite photocatalysts have shown a promising VL photocatalytic performance to the decomposition

Received: March 18, 2013
Accepted: July 10, 2013
Published: July 10, 2013

   dx.doi.org/10.1021/am401459c | ACS Appl. Mater. Interfaces 2013, 5, 6959−6967

of organics. It has been reported that the Ag/AgI@Al_2O_3-supported plasmon-induced photocatalyst possesses much higher photocatalytic stability and activity than those of the bare Ag/AgI photocatalyst for the decomposition and mineralization of the toxic organics.[14] Another recent work report also indicated that a nanocomposites made of Ag/AgX loaded graphene oxide (GO) (Ag/AgX@GO) has significantly enhanced photocatalytic activity and stability as compared to those of bare Ag/AgX (X = Cl, Br) plasmonic photocatalysts.[16] These research findings imply that the photocatalytic activity as well as the stability of Ag/AgX can be significantly enhanced by loading onto a suitable supporting material.

Recently, carbon nanotubes (CNTs) have attracted a considerable interest because of their excellent mechanical, electrical, and chemical properties. It has been frequently employed as a catalyst carrier because of its hollow and layered structure as well as large specific surface area with superior adsorption properties toward organic pollutants. In addition, CNTs can serve as an electron reservoir to reduce the electron−hole recombination.[7,21,22] Also, CNTs can act as a dispersing template, affecting the structure and morphology of TiO_2 formed on the CNTs, which in turn can improve the performance of the resultant composite photocatalysts.[23−25] More recently, a novel micrometer-sized CNTs−natase TiO_2 sphere photocatalyst was hydrothermally synthesized for efficient removal of gaseous organic pollutants by our group,[26] and the results further confirmed the synergistic and beneficial effects in improving the photocatalytic activity can be due to the CNTs supporter. Xin et al recently reported the use of Ag-CNTs as filters to prepare polypropylene (PP) and polystyrene (PS) nanocomposites. Their results showed that the mechanical property as well as electrical conductivity of PP and PS have been enhanced effectively due to addition of Ag-CNTs.[27] Another study also showed that Ag-deposited CNTs can be used in various polymeric nanocomposites and coatings to increase the UV reflection properties.[28] However, as known, the synthesis VL active Ag/AgX-CNTs nanocomposite photocatalyst based on plasmon-induced VLD photocatalysis has not been previously reported.

In this study, to collectively utilize the advantageous properties of CNTs and Ag/AgX, a series of CNTs-based Ag/AgX-CNTs (X = Cl, Br, I) nanocomposite plasmonic photocatalysts with high VL activities were fabricated via a facile ultrasonic-assisted precipitation method. It is well-known that 2,4,6-tribromophenol (TBP) is a frequently used brominated flame retardants (BFRs) employed to retard fire risk for production of electronic devices, plastics, epoxy, paper, and polyurethane. It might possess estrogen-like property and has strong potential for developmental fetotoxicity, embryotoxicity, and neurotoxicity. Also, it can be detected in human plasma and a wide range of environmental samples due to its bioaccumulation and persistent property. Therefore, TBP was selected as a model BFR to study the photocatalytic performance of the newly synthesized photocatalysts. The results demonstrate that the fabricated Ag/AgX-CNTs nanocomposite photocatalysts possess a dramatically improved VL catalytic degradation efficiency toward TBP as compared to the unsupported Ag/AgX photocatalysts. In this study, the synergetic effect of Ag/AgX-CNTs to enhance the VLD photocatalytic degradation efficiency pave an way to develop new generation VL active photocatalysts.

EXPERIMENTAL SECTION

Preparation of Ag/AgX-CNTs (X = Cl, Br, I) Photocatalysts. One gram of multiwall CNTs (MWCNTs) with length of 5−15 μm and the diameter of 60−100 nm (Shenzhen Nanotech Port Co., Ltd., China) was first pretreated by refluxing in a 40 mL mixture of concentrated nitric acid (65−68%) and sulphuric acid (95−98%) with a volume ratio of 1:3 at 90 °C for 90 min. Then the backup CNTs were achieved after the sequence filtration, washing with distilled water and then drying at 80 °C.

Ag/AgX-CNTs (X = Cl, Br, I) photocatalysts were prepared by an ultrasonic assistant deposition-precipitation method. For a typically synthesis procedure, 1.5 mmol of KX (X= Cl, Br, I) was dissolved into 30 mL ultrapure Milli-Q water (Electrical conductivity is 17 S cm^{-1}), and 0.2 g of purified CNTs was added into the suspension. The resultant mixture was first homogenized by ultrasonication for 20 min in a ultrasonic cleaner (Ningbo Yinzhou Yongjie experimental instrument Co., LTD, YJ-5200D, frequency: 40kHz), and then the mixture of 1.5 mmol of $AgNO_3$ and ammonia solution (2.5 mL, 25 wt % NH_3) was added dropwise into the above homogeneous solution. Here, the ammonia solution serves both as a complex reagent for Ag^+ and controlling solution pH to enabling the control of the rate of formation of AgX (X = Cl, Br, I) and preventing the agglomerate of synthesized AgX. The resultant solution was ultrasonicated for another 20 min before being stirred for 24 h, and then the resultant mixture was washed with Milli-Q water three times, and dried at 70 °C.

Characterization. To clarify the crystal phase composition of the prepared photocatalysts, we measured X-ray diffraction (XRD) was measured using a Rigaku Dmax 2200 V X-ray diffractometer, and the specific surface area, average pore diameter and specific pore volume of the photocatalysts were determined by nitrogen adsorption−desorption isotherms using an ASAP 2020 sorption analyzer. Images were obtained on a scanning electron microscopy (SEM, JSM-6330F). The UV−vis absorption spectra (UV−vis) were measured with a UV-2501PC UV−vis spectrophotometer. The X-ray photoelectron spectroscopy (XPS) analyses of the samples were carried out on an S-520/INCA 300 spectrometer using 300W Mg−Kα radiation, and the binding energies were referenced to the C1s line at 284.8 eV from adventitious carbon. To measure the redox properties of the prepared photocatalysts, we investigated the temperature-programmed reduction (TPR) and the temperature-programmed oxidation (TPO) on a TP-5078 multifunction adsorption instrument (Tianjin, China).

Photocatalytic Activity. The photocatalytic activity of the resultant photocatalysts was evaluated by the removal of TBP in water under VL irradiation. The schematic diagram of the experimental setup is shown in Figure S1 in the Supporting Information. The photocatalytic reactor is a 150 mL quartz bottle with a water-jacket outside. In a typical performance, 30 mg of photocatalyst was dispersed in 50 mL of 100 μmol L^{-1} TBP solution (pH 10). The light source was a 250 W metal-halide lamp (PLS-SXE300, Shanghai Bilang Co., Ltd., China) with a UV cutoff filter (λ < 400 nm) and the illumination intensity was kept at ca. 5 mW cm^{-2} (the spectrum of light source with the UV cutoff filter was presented in Figure S2 in the Supporting Information). In all experiments, the temperature of the reaction was maintained at 25 ± 1 °C by the water continuously circulated in the jacket surrounding the reactor. Before irradiation, all the reaction samples were stirred for 30 min in dark to obtain an adsorption−desorption equilibrium. The dark adsorption time was set as 30 min because there was insignificant change in the TBP adsorption after 30 min (see Figure S3 in the Supporting Information). Once the TBP concentration has stabilized, the solution was then illuminated with VL to start the photocatalysis. Afterward, aliquots (1.5 mL) of dispersion were collected and filtered using a 0.22 μm Millipore filter for further analysis at regular intervals of irradiation time, and the TBP concentration was detected by using a Agilent 1200 high pressure liquid chromatography (HPLC) equipped with a DAD detector.[29] For the assessment of photocatalytic activities of resultant photocatalyst, the degradation efficiency = $C/C_0 \times 100\%$ was used, where C and C_0 is the concentrations of TBP at a real-time t and the initial concentration of TBP. For comparison, light (without

photocatalyst) and dark controls (without light) were also performed. All the aforementioned experiments including controls were also conducted in triplicates.

RESULTS AND DISCUSSION

Characterization of Photocatalysts. *Morphology and Structure.* To obtain the microscopic morphology and structural characteristics, SEM analyses of the prepared Ag/AgX-CNTs (X = Cl, Br, I) nanocomposites and the unsupported AgX are preformed. The obtained morphologies of AgCl and AgBr particles are irregular sphere-like (Figure 1a,c) with a diameter distribution ranging 1−5 μm. The average

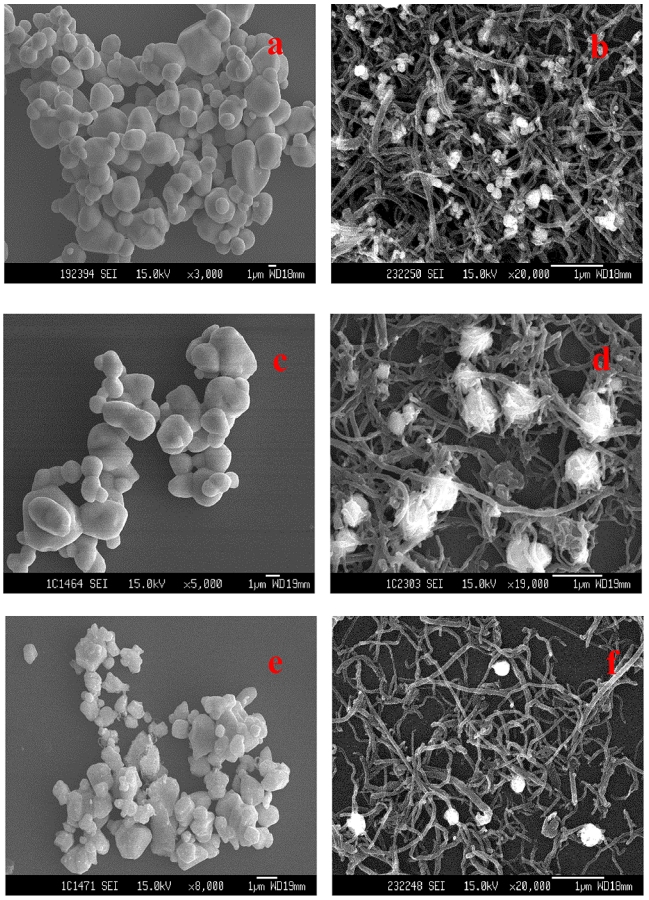

Figure 1. Typical SEM images of (a) AgBr, (b) Ag/AgBr-CNTs, (c) AgCl, (d) Ag/AgCl-CNTs, (e) AgI, and (f) Ag/AgI-CNTs.

particle size of AgCl is bigger than that of AgBr. The AgI sample shows irregular blocky particles (Figure 1e) with rougher surfaces compared to that of AgCl and AgBr. When CNTs was added as the supporter of AgX, well-dispersed Ag/AgX particles are clearly scattered on the surface of pretreated CNTs supporter with average ranged from 300 to 500 nm (Figure 1b, d, and f). Moreover, the average diameter of Ag/AgBr is smaller than those of Ag/AgI and Ag/AgCl in the Ag/AgX/CNTs. Compared with their corresponding AgX particles, smaller size of AgX nanospheres are found in Ag/AgX-CNTs composites because of the presence of CNTs supporter in these composites, confirming the beneficial role of CNTs in control growth of AgX particles. Recently, it has been certified that the acid-treated CNTs possess excellent hydrophilic properties.[30] This can be used to further improve the dispensability of Ag/AgX in aqueous phase and prevent the aggregation of Ag/AgX particles.

XRD and XPS Analysis. The phase structure of the resultant Ag/AgX-CNTs (X = Cl, Br, I) nanocompsites were analyzed by XRD. Figure 2a demonstrates the XRD patterns of bare CNTs,

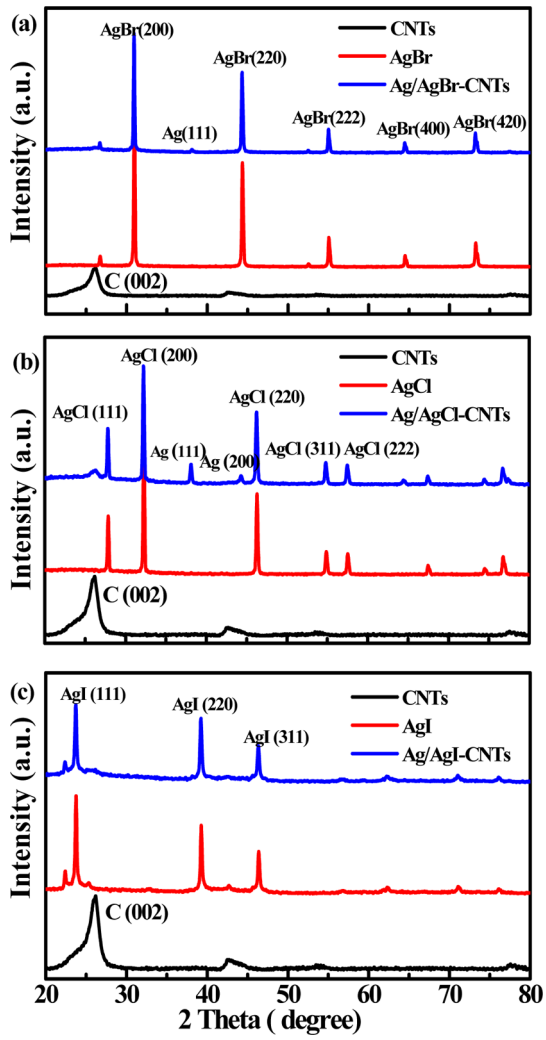

Figure 2. XRD spectra of (a) CNTs, AgBr, and Ag/AgBr-CNTs; (b) CNTs, AgCl, and Ag/AgCl-CNTs; and (c) CNTs, AgI, and Ag/AgI-CNTs.

as-prepared AgBr and Ag/AgBr-CNTs. The as-prepared Ag/AgBr-CNTs are mainly AgBr cubic phase. The peaks at 2θ values of 30.8, 44.2, 55.1, 64.5, and 73.2° match very well with the diffraction peaks of (200), (220), (222), (400), and (420) crystal planes of AgBr (JPCDS file, 06−0438), respectively. Both characteristic diffraction peaks of CNTs (002) (JCPDS file, 41−1487) at 26.2°, and Ag (111) (JCPDS file, 65−8428) facets at 37.8° are observed. Similar results are also obtained for Ag/AgCl-CNTs (Figure 2b). That is, the as-prepared Ag/AgCl-CNTs consist of CNTs (26.2°), and AgCl (JCPDS file, 31−1238) (27.8, 32.3, 46.3, 54.9, 55.6, 67.4, 74.4, and 76.8°) as well as a spot of metallic Ag (38.1, 44.4, and 64.4°). For Ag/AgI-CNTs (Figure 2c), the peaks in the XRD patterns are characterized as AgI (JCPDS file, 09−0388) (23.6, 39.1, and 46.4°) and CNTs. Nevertheless, unlike Ag/AgBr-CNTs and Ag/AgCl-CNTs, no obvious metallic Ag diffraction peak is observed in the XRD pattern of Ag/AgI-CNTs photocatalyst.

dx.doi.org/10.1021/am401459c | ACS Appl. Mater. Interfaces 2013, 5, 6959−6967

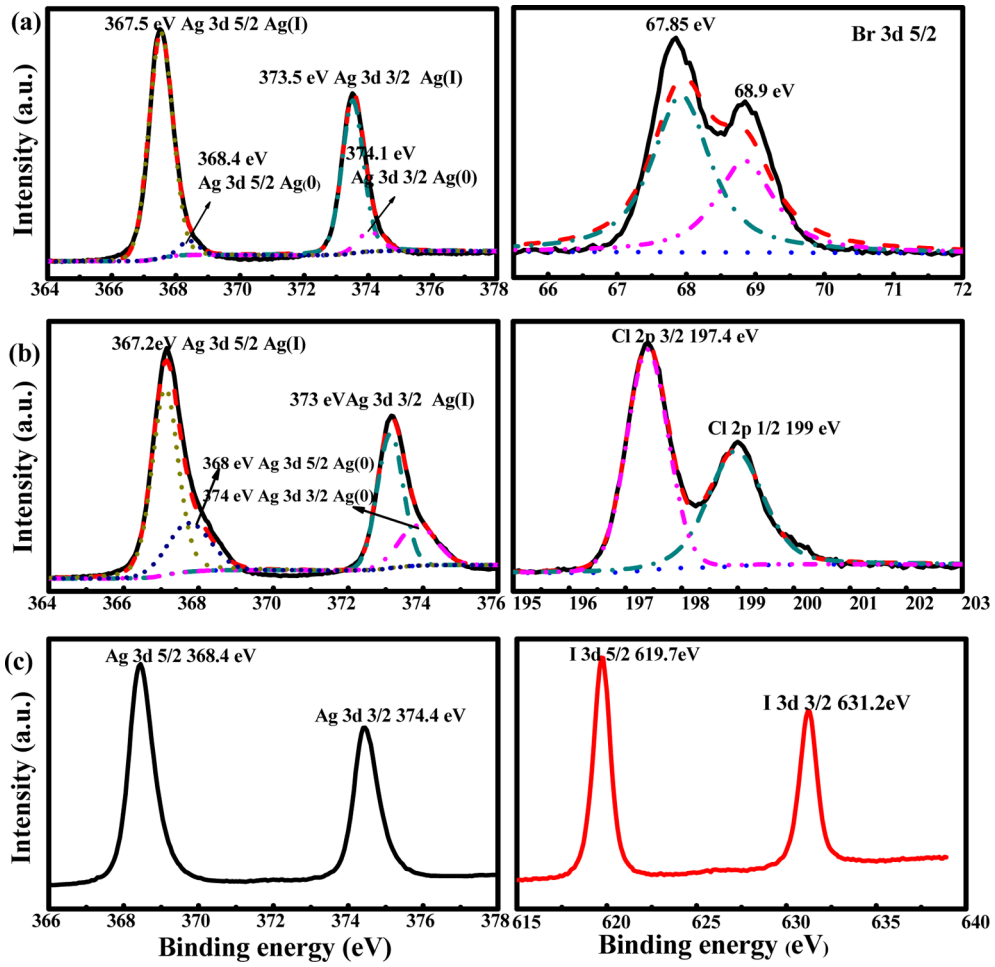

Figure 3. XPS spectra of Ag 3d and X 3d (X = Cl, Br, I) in (a) Ag/AgBr-CNTs, (b) Ag/AgCl-CNTs, and (c) Ag/AgI-CNTs.

To verify the hybridization structure of Ag/AgX-CNTs (X = Cl, Br, I), the surface elemental compositions of the as-prepared photocatalysts were further characterized by XPS (Figure 3). Figure 3a illustrates the XPS data for Ag/AgBr-CNTs. The two bands observed at ca. 367.5 and 373.5 eV can be ascribed to Ag3d 5/2 and Ag3d 3/2 binding energies, respectively. Each of these bands can be further divided into a pair of peaks (367.5/368.4 eV, and 373.5/374.1 eV). The first pair of bands at 367.5 and 373.5 eV is attributed to Ag(I) of AgBr, whereas the second pair of bands at 368.4 and 374.1 eV is ascribed to the metallic Ag(0). Similar results were also obtained by a number of previous studies.[4,16,18] These observations confirm the existence of metallic Ag(0) on the surface of Ag/AgBr-CNTs, which is well -consistent with XRD analysis results. As for Br 3d spectra (Figure 3b), two individual peaks, Br 3d5/2 and Br 3d3/2 with the binding energies of 68.85 and 68.9 eV, respectively, were also obtained, indicating the presence of Br^-.[18,31]

Similar results were also obtained for Ag/AgCl-CNTs (Figure 3b). That is, two observed bands at 367.2 and 373.0 eV can be ascribed to Ag 3d5/2 and Ag 3d3/2 binding energies, respectively, each be further divided into a pair of peaks (367.2/368.0 eV, and 373.0/374.0 eV). The former bands at 367.2 and 373.0 indicate the presence of Ag(I), whereas the latter bands at 368.0 and 374.0 eV suggest the existence of the metallic Ag(0). However, for the Ag/AgI-CNTs photocatalyst (Figure 3c), the peaks at 368.4 and 374.4 eV originated only from Ag(I) of AgI, but no metallic Ag(0) diffraction peaks are observed.

UV–Vis Analysis. UV–vis absorption spectra of photocatalysts reflect their ability to harvest the solar radiation and can be used to calculate the band gap energy. Generally, the bare AgX (X = Cl, Br, I) samples could exhibit distinct adsorption only in the UV region but limited in the VL region.[13,16,32,33] However, the Ag/AgBr-CNTs photocatalyst has apparent absorption intensity in VL region with a significant enhancement (Figure 4a). Similar results were also obtained for Ag/AgCl-CNTs and Ag/AgI-CNTs (Figure 4b, c). Under the VL irradiation, the reduced Ag(0) species nucleate on the surface of AgX nanoparticle and form dispersed Ag nanograins, which would arouse strong plasmon resonance absorptions in VL region.[1,16,20] Thus, it can be inferred that the presence of CNTs can improve the VL adsorption of the resultant Ag/AgX-CNTs composite photocatalysts although the UV adsorption of bare AgX nanoparticles was very limited. Similar result was also obtained by Wang's report.[34] The band gap energies of different AgX were computed and presented in Table 1. The band gap of AgBr is obtained as 2.69 eV, which is smaller than those of AgCl (2.90 eV) and AgI (2.88 eV). This means that the Ag/AgBr-CNTs photocatalyst may be readily excited by a wide range of VL as compared to other Ag/AgX-CNTs photocatalysts.

H_2-TPR and O_2-TPO Analysis. The H_2-TPR and O_2-TPO technologies were used to characterize the redox ability of the

dx.doi.org/10.1021/am401459c | ACS Appl. Mater. Interfaces 2013, 5, 6959–6967

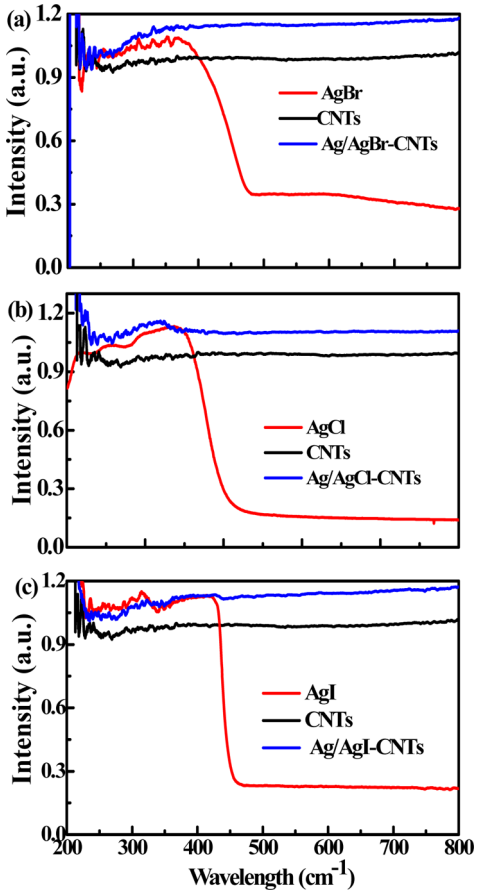

Figure 4. UV−vis spectra of (a) Ag/AgBr-CNTs, (b) Ag/AgCl-CNTs, and (c) Ag/AgI-CNTs.

Table 1. Textural Parameters of the As-Prepared Photocatalysts

	SSA_{BET} (m^2 g^{-1})	pore diameter (nm)	pore volume (cm^3 g^{-1})	E_g[a] (eV)
AgCl	2.5		0.005	2.92
AgBr	1.4		0.001	2.69
AgI	0.7		0.0007	2.87
CNTs	59.2	15.6	0.245	
Ag/AgCl-CNTs	50.3	16.8	0.289	
Ag/AgBr-CNTs	20.8	26.0	0.142	
Ag/AgI-CNTs	18.4	35.9	0.159	

[a] E_g was derived from $E_g = 1240/\lambda_g$, where λ_g is the absorption edge in the UV−vis spectra

resultant photocatalysts. From the H_2-TPR profiles, a strong H_2 consumption peak was found for all these prepared Ag/AgX-CNTs photocatalysts (Figure 5), attributing to the reduction of Ag(I) to the metallic Ag(0).[35−37] Moreover, it is interesting to find that the obtained reduction temperatures of the bare AgCl, AgBr and AgI are found to be at 622, 753, and 882 °C, respectively, which are higher than those for AgX in the Ag/AgCl-CNTs (445 °C), Ag/AgBr-CNTs (565 °C) and Ag/AgI-CNTs (784 °C) composite photocatalysts. So it can be inferred that the presence of CNTs can lower the reduction temperature of the resultant composite photocatalysts. This is because, with addition of CNTs, the storage ability of H_2 is enhanced, and then the density of H_2 increases on the surface of catalyst. Subsequently the reduction ability is enhanced, leading to a decrease in the reduction temperature. As such, the reduction temperature of AgX in the Ag/AgCl-CNTs is lower than those of others. The order of the reduction temperature is Ag/AgCl-CNTs < Ag/AgBr-CNTs < Ag/AgI-CNTs, which is in good agreement with the reduction order of AgX and is as opposed to the redox potential of AgCl (0.22 V) > AgBr (0.10 V) > AgI (−0.15 V). That is, the higher of the redox potential, the more of Ag(0) particles presence, even with the same photons excited. In addition, the amount of H_2 consumption for the Ag/AgCl-CNTs, Ag/AgBr-CNTs and Ag/AgI-CNTs are 17.69, 30.34, and 15.19 mmol g^{-1}, respectively. This may suggest that more active centers are existed on the Ag/AgBr-CNTs surface than other two photocatalysts. Therefore, compared to Ag/AgCl-CNTs and Ag/AgI-CNTs,[35] better reduction ability and the photocatalytic activity can be expected for Ag/AgBr-CNTs.

Figure 6 shows the O_2-TPO profiles of the as-prepared Ag/AgX-CNTs photocatalysts as well as CNTs as the control. Only one oxidative peak is observed for all photocatalysts investigated, while for CNTs, a gradually increased intensity signal without oxidation peak was obtained.[38] This oxidative peak may attribute to the oxidation reaction of Ag(0) to Ag_2O, which further confirms the existence of Ag(0) in all Ag/AgX-CNTs samples. The oxidation peak temperatures of Ag/AgCl-CNTs, Ag/AgBr-CNTs, and Ag/AgI-CNTs photocatalysts are 550, 549, and 516 °C, respectively, indicating that the oxidation temperature of Ag/AgI-CNTs is the lowest among the three photocatalysts. Therefore, it can be concluded that the Ag(0) indeed existed in the Ag/AgI-CNTs with limited amounts even though the amount of Ag(0) can not be detected by XPS and XRD.

BET Surface Area and Pore Distribution. The plot of N_2 adsorption−desorption isotherms as well as pore size distribution plot of the Ag/AgX-CNTs (X = Cl, Br, I) photocatalysts are given in Figure S4 in the Supporting Information. All the isotherms can be ascribed to type IV curve with H3 hysteresis loop, suggesting the existence of mesoporous pore structures.[29,39] The pore size distribution plots (inset of Figure S4 in the Supporting Information) of these photocatalysts exhibit a wide pore size distribution ranged from 20 to 60 nm. In addition, the textural parameters of the prepared photocatalysts are summarized in Table 1. For the samples without addition of CNTs, the obtained specific surface areas of pure AgCl, AgBr and AgI are only 2.5, 1.4, and 0.7 m^2 g^{-1}, respectively. When CNTs were added as a supporter of AgX, the specific surface area of Ag/AgCl-CNTs, Ag/AgBr-CNTs and Ag/AgI-CNTs are increased to 50.3, 20.8, and 18.4 m^2 g^{-1}, respectively. Meanwhile, the obtained pore volumes of Ag/AgX-CNTs are 0.289, 0.142, and 0.159 cm^3 g^{-1}, respectively, which are also larger than those of corresponding AgX (X = Cl, Br, I). That is, the specific surface areas and pore volumes of Ag/AgCl-CNTs are significantly enhanced due to the input of large specific surface area by CNTs, leading to a significantly enhanced adsorption capability and transfer ability of organic pollutants onto the photocatalyst to enhance the catalytic activity.[40]

Photocatalytic Activity and Mechanism. The dark experiment (adsorption) and blank experiment (photolysis) were first carried out and the degradation of TBP could be neglected in both cases (Figure 7a). The photocatalytic degradation of TBP by bare CNTs, AgBr, and the as-prepared Ag/AgBr-CNTs composites were investigated under VL

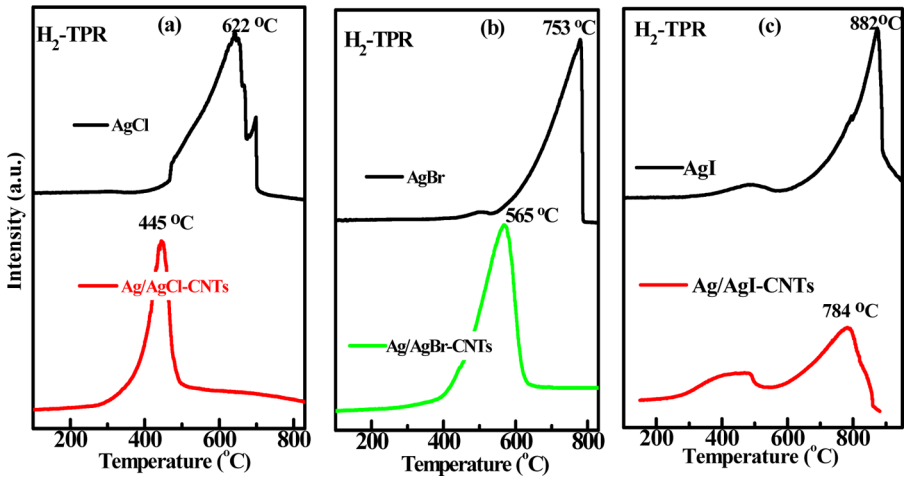

Figure 5. H_2-TPR spectra of (a) AgCl and Ag/AgCl-CNTs, (b) AgBr and Ag/AgBr-CNTs, and (c) AgI and Ag/AgI-CNTs.

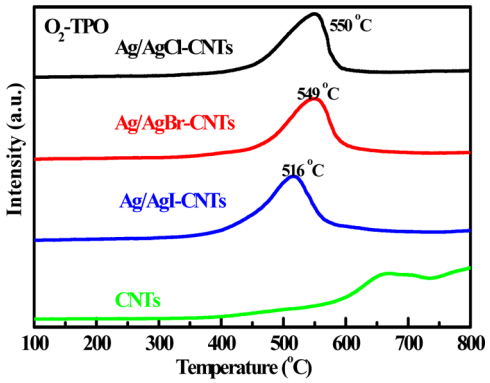

Figure 6. O_2-TPO spectra of Ag/AgCl-CNTs, Ag/AgBr-CNTs, Ag/AgI-CNTs, and pure CNTs.

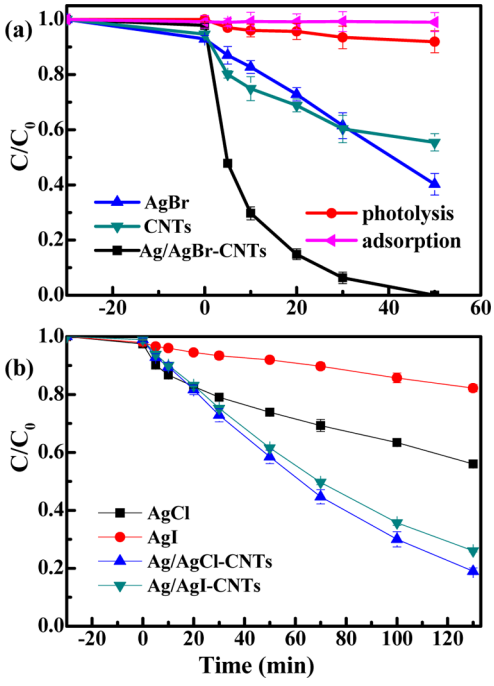

Figure 7. Photocatalytic activity of prepared catalysts for degradation of TBP under visible-light irradiation.

illumination (Figure 7a). 100% of 100 μmol L^{-1} TBP can be photocatalytically degraded within 50 min when Ag/AgBr-CNTs was used as the photocatalyst under VL irradiation. In contrast, under the same experimental conditions, only 60 and 45% of TBP are decomposed when AgBr or CNTs is employed as photocatalyst, respectively. Furthermore, the effect of the amount of AgBr was studied (see Figure S5 in the Supporting Information). The Ag/AgBr-CNTs photocatalyst exhibits an excellent photocatalytic activity when the amount of AgBr is 1.5 mmol, because the excess AgBr will aggregate on the surface of CNTs, resulting in a reduced photocatalytic performance. The modest photocatalytic activity of CNTs could be due to the ability of CNTs to produce the reactive oxygen species (ROSs) under irradiation.[41] Apparently, the photocatalytic activity of Ag/AgBr-CNTs is markedly improved by the loading of AgBr onto the CNTs surface.

The photocatalytic removal of TBP was also performed using Ag/AgCl-CNTs and Ag/AgI-CNTs as photocatalysts (Figure 7b). Only 39 and 42% of the TBP can be degraded using Ag/AgCl-CNTs and Ag/AgI-CNTs, respectively. As a comparison, only 26 and 8% of TBP were degraded by corresponding pure AgCl and AgI without CNTs, respectively. Further prolonging the reaction time to 130 min, 82, 74, 44, and 18% of TBP degradation can be achieved with Ag/AgCl-CNTs, Ag/AgI-CNTs, AgCl and AgI as photocatalysts, respectively. These results further validate that for photocatalytic degradation of TBP, Ag/AgX-CNTs (X = Cl, Br, I) composite photocatalysts possess better photocatalytic activity than pure AgX. Among all catalyst investigated in this work, the Ag/AgBr-CNTs displays the highest photocatalytic activity. It may be because that the particle size of Ag/AgBr-CNTs is smaller than that of Ag/AgCl-CNTs and Ag/AgI-CNTs (Figure 1), that benefits the photocatalytic performance enhancement.[29] As demonstrated by the data in Figure 5, the highest H_2 consumption by Ag/AgBr-CNTs may imply more active sites on the catalyst surface.

It is important to understand the photocatalytic degradation mechanism of plasmonic photocatalysts such Ag/AgBr-CNTs. As a hybrid composite, the electronic band structures of individual components is critical for the photocatalytic performance, which determine the excitation, transportation, and the recombination of the photogenerated electron−hole pairs.[42,43] To investigate the photocatalytic mechanism of Ag/AgBr-CNTs, first of all, it is necessary to know the band structure of the AgBr phase. Therefore, the conducting band

dx.doi.org/10.1021/am401459c | ACS Appl. Mater. Interfaces 2013, 5, 6959−6967

(CB) and valence band (VB) energies of the AgBr are calculated to be about −0.065 and +2.625 V (vs SHE), respectively.[4] It is reported that the plasmon-induced electrons of metallic Ag nanoparticles can transfer to the CB (−0.2 V vs SHE) of TiO_2 anatase under VL illumination.[44] So it is possible that the plasmon-induced electrons at Ag nanoparticles of Ag/AgBr-CNTs with a strong reduction power can readily transfer to CB (−0.065 V vs SHE) of AgBr. As depicted in Scheme 1,

Scheme 1. Schematic Drawing of the Photocatalytic Process with Ag/AgBr-CNTs Composite Photocatalyst

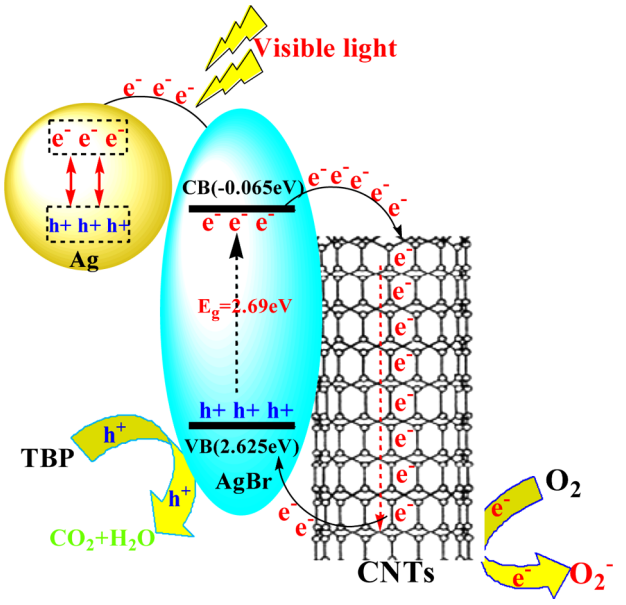

when the photocatalyst is subjected to the VL irradiation, the photosensitive AgBr in Ag/AgBr-CNTs composite can be decomposed into Ag(0), and Ag(0) is subsequently excited by VL due to the localized surface plasmon resonance to generate electron−hole pairs on the Ag nanoparticle surface.[1,4,14,16] Simultaneously, the AgBr can also be excited by VL to generate the electron−hole pairs. Therefore, the possible photocatalytic mechanism of Ag/AgBr-CNTs could be described as that the plasmon-induced e^- at Ag nanoparticles transfers to the CB_{AgBr}, and then the two parts of e^- on CB_{AgBr} would prefer flowing down to the CNTs, while the plasmon-induced h^+ remains on the surface of Ag and AgBr to oxidize organic pollutant. Such transportation of the photogenerated charge carriers could either stabilize the photogenerated h^+ in the VB_{AgBr} or prolong their transfer path, resulting in extending the lifetime of the charge carriers and effectively suppressing the unfavorable charge recombination.[45] The VB_{AgBr} (2.625 eV) is more positive than the standard redox potential of •OH/OH (1.99 eV), suggesting the photogenerated holes possess higher oxidative power than •OH.[42]

On the basis of the above discussions, the photocatalytic degradation mechanism of TBP using Ag/AgBr-CNTs as photocatalyst could be presented as eqs 1−6. It is supposed that under VL irradiation, the photocalaysts is first excited to generate e^- at the CB of the AgBr. The CB e^- would then react with Ag(I) to form Ag(0). The formed Ag(0) could also be excited by VL due to the strong plasma resonance effect (eqs 2 and 3). On the other hand, the CB e^- could react with soluble O_2 to produce reactive O_2^-• (eq 4). Correspondingly, h^+ was left on VB. The photocatalytically produced h^+ (eq 1) and O_2^-• (eq 4) possess strong oxidation power to readily decompose a wide spectrum of hazardous organics, including TBP, into intermediates (eqs 5 and 6).

$$\text{Ag/AgBr-CNTs} \xrightarrow{h\nu} e_{CB}^- + h_{VB}^+ \quad (1)$$

$$\text{Ag(I)} + e^- \rightarrow \text{Ag(0)} \quad (2)$$

$$\text{Ag(0)} \xrightarrow{h\nu} \text{Ag(I)} + e^- \quad (3)$$

$$e_{CB}^- + O_2 \rightarrow O_2^- \quad (4)$$

$$\text{TBP} + h_{VB}^+ \rightarrow \text{intermediates} \quad (5)$$

$$\text{TBP} + O_2^- \rightarrow \text{intermediates} \quad (6)$$

Furthermore, the superior e^- mobility of CNTs supporter of these photocatalysts facilitates e^- transport to enhance the electron−hole separation. Indeed, the efficient e^- transfer from plasmon-induced Ag(0) nanoparticles to CNTs also enhance the stability of Ag/AgBr-CNTs composites by maintaining the plasmon-excited e^- away from AgBr, avoiding the electrons being trapped by Ag^+ in AgBr, thus prevents the AgBr decomposition during photocatalytic process. Therefore, the high photocatalytic activity and modest stability of Ag/AgBr-CNTs are ensued. Besides the enhancement of charge separation, the photocatalytic reaction also involves in the transportation of organic molecules onto the surface of catalyst to speed up the photocatalytic degradation of organics.[1] Since the giant π-conjugation between CNTs and TBP molecules, CNTs would adsorb TBP molecules from the solution, and thus facilitate the photocatalytic degradation of TBP at the catalyst surface.[46] The band gap of AgCl and AgI are also obtained as 2.92 and 2.86 eV, respectively, which is quite close to that of AgBr. So the photocatalytic mechanism of other photocatalysts should be similar to Ag/AgBr-CNTs.

Deactivation Mechanism of Used Photocatalysts. The deactivation of Ag/AgBr-CNTs photocatalyst was also evaluated by repeatedly performing 5 times of the TBP degradation experiments using same catalyst (see Figure S6 in the Supporting Information). Gradually decreased TBP degradation efficiencies from 100 to 83% was obtained from the second to fifth reuse cycles of the photocatalyst under 80 min VL irradiation. Such a slightly decreased activities within 5 resuse cycles suggests a modest stability of Ag/AgBr-CNTs.[16,17,32] The modest stability of Ag/AgBr-CNTs could be due to the supporting effect of CNTs for AgBr photocatalyst. It is well-known that an effective charge separation and transfer is important for photocatalytic activity improvement.[47,48] Therefore, it is sound to believe that a reinforced charge transfer and separation could be obtained in Ag/AgBr-CNTs hybrid nanocomposites, where Ag/AgBr and CNTs might act as e^- donor and e^- acceptor, respectively.[16]

Although this newly prepared photocatalyst is relatively efficient for degradation of TBP and stable under VL, the deactivation mechanism of the photocatalyst should be investigated. The slight reduce of the photocatalytic performance during the photocatalyst recycling reactions could be the loss of small part of Ag^+ on the photocatalyst surface during light irradiation, since Ag^+ could be reduced to metallic Ag(0) by photogenerated e^-, which can be verified by XRD and XPS analyses of prepared photocatalyst after reuse. As clearly displayed in Figure S7 in the Supporting Information, the reused Ag/AgBr-CNTs photocatalyst exhibits similar XRD

dx.doi.org/10.1021/am401459c | ACS Appl. Mater. Interfaces 2013, 5, 6959−6967

patterns as the virgin phootocatalyst, suggesting the general phase structure of the used photocatalyst is very stable and unchanged. However, the diffraction intensity of AgBr decreased slightly with the increased of the reusing times of photocatalyst. In contrast, the diffraction intensity of Ag(0) increases slightly, and two other observed diffraction peaks located at 37.8 and 77.2° indexed to the phase of Ag(111) and Ag(311) facets are obvious, suggesting that part of Ag^+ has been reduced to metallic Ag(0) on the catalyst surface.[18,31]

To further confirm this observation, XPS patterns of photocatalyst after 5-reused cycles were investigated during the degradation of TBP under VL irradiation (see Figure S8 in the Supporting Information). The peak intensity of metallic Ag(0) at ca. 368.5 and 374.6 eV are slightly higher for fifth reused Ag/AgBr-CNTs photocatalyst than those of fresh and reused once only once (see Figure S8 in the Supporting Information). The ratio of Ag(I):Ag(0) is 2.94 in the fresh Ag/AgBr-CNTs composite and decreased to 1.68 after one cycle of reuse, and further decreased to 1.08 after 5 cycles of reuse. That is, from the XRD and XPS data, it can be confirmed that the amount of Ag(0) increased as the reused cycle number increased. Furthermore, the binding energy of Br 3d 5/2 was shifted nearly 1 eV to higher energy as the reused cycle number increased. This is also due to the reduction of Ag^+ to metallic Ag(0), leading to slightly changing the chemical environment of Br^- on the photocayalyst surface, hence decreases the electron density of surrounding Br^-.

CONCLUSIONS

In summary, Ag/AgX (X = Cl, Br, I) loaded CNTs nanocomposite photocatalysts with high activity have been successfully prepared via an ultrasonic assistant deposition-precipitation method at room temperature. The Ag/AgX-CNTs (X = Cl, Br, I) exhibit excellent photocatalytic activity due to the enhancement of photogenerated charge-hole pairs separation and transportation from plasmon-excited Ag(0) nanoparticles. The order of VLD photocatalytic activity is Ag/AgBr-CNTs > Ag/AgCl-CNTs > Ag/AgI-CNTs. Among them, the Ag/AgBr-CNTs exhibit the best photocatalytic activity and modest stability. The results indicate that the as-prepared photocatalysts have potential application in the abatement of organic pollutants in water. As far as we know, this is the first work about the assembly of CNTs with plasmonic Ag(0) photocatalysts. The investigation can open a new opportunity to develop novel CNTs-based photocatalysts involved in plasmonic effect that utilize visible light to decompose harmful organics.

ASSOCIATED CONTENT

Supporting Information

Schematic diagram of the reactor, Xenon lamp spectrum with UV cutoff filter, the adsorption−desorption equilibrium of TBP, N_2 adsorption−desorption isothermal plots, as well as multicycle run of photocatalytic degradation of TBP over Ag/AgBr-CNTs. This material is available free of charge via the Internet at http://pubs.acs.org.

AUTHOR INFORMATION

Corresponding Author

*E-mail: antc99@gig.ac.cn. Tel: +86-20-85291501. Fax: +86-20-85290706.

Notes

The authors declare no competing financial interest.

ACKNOWLEDGMENTS

This is contribution IS−1608 from GIGCAS. This work was supported by the Team Project of the Natural Science Foundation of Guangdong Province, China (S2012030006604), NSFC (21077104), the Science and Technology Project of Guangdong Province, China (2012A032300010 and 2011A030700003), and China Postdoctoral Science Foundation (2012M511843).

REFERENCES

(1) Zhang, H.; Fan, X. F.; Quan, X.; Chen, S.; Yu, H. T. *Environ. Sci. Technol.* **2011**, *45*, 5731−5736.
(2) Xiong, Z. G.; Zhao, X. S. *J. Am. Chem. Soc.* **2012**, *134*, 5754−5757.
(3) Tsukamoto, D.; Shiraishi, Y.; Sugano, Y.; Ichikawa, S.; Tanaka, S.; Hirai, T. *J. Am. Chem. Soc.* **2012**, *134*, 6309−6315.
(4) Wang, X. F.; Li, S. F.; Ma, Y. Q.; Yu, H. G.; Yu, J. G. *J. Phys. Chem. C* **2011**, *115*, 14648−14655.
(5) Li, G. Y.; Liu, X. L.; Zhang, H. M.; An, T. C.; Zhang, S. Q.; Carroll, A. R.; Zhao, H. J. *J. Catal.* **2011**, *277*, 88−94.
(6) Shi, H. X.; Zhang, T. Y.; Li, B.; Wang, X.; He, M.; Qiu, M. Y. *Catal. Commun.* **2011**, *12*, 1022−1026.
(7) Chen, J. Y.; Li, G. Y.; Huang, Y.; Zhang, H. M.; Zhao, H. J.; An, T. C. *Appl. Catal. B* **2012**, *123−124*, 69−77.
(8) Primo, A.; Marino, T.; Corma, A.; Molinari, R.; Garcia, H. *J. Am. Chem. Soc.* **2011**, *133*, 6930−6933.
(9) Le, T. T.; Akhtar, M. S.; Park, D. M.; Lee, J. C.; Yang, O. B. *Appl. Catal. B* **2012**, *111−112*, 397−401.
(10) Sun, S. M.; Wang, W. Z.; Zhang, L.; Zhou, L.; Yin, W. Z.; Shang, M. *Environ. Sci. Technol.* **2009**, *43*, 2005−2010.
(11) Wang, D. F.; Kako, T.; Ye, J. H. *J. Phys. Chem. C* **2009**, *113*, 3785−3792.
(12) Wang, D. F.; Kako, T.; Ye, J. H. *J. Am. Chem. Soc.* **2008**, *130*, 2724−2725.
(13) Wang, P.; Huang, B. B.; Zhang, Q. Q.; Zhang, X. Y.; Qin, X. Y.; Dai, Y.; Zhan, J.; Yu, J. X.; Liu, H. X.; Lou, Z. Z. *Chem.—Eur. J.* **2010**, *16*, 10042−10047.
(14) Hu, C.; Peng, T. W.; Hu, X. X.; Nie, Y. L.; Zhou, X. F.; Qu, J. H.; He, H. *J. Am. Chem. Soc.* **2009**, *132*, 857−862.
(15) Awazu, K.; Fujimaki, M.; Rockstuhl, C.; Tominaga, J.; Murakami, H.; Ohki, Y.; Yoshida, N.; Watanabe, T. *J. Am. Chem. Soc.* **2008**, *130*, 1676−1680.
(16) Zhu, M. S.; Chen, P. L.; Liu, M. H. *ACS Nano* **2011**, *5*, 4529−4536.
(17) Yu, J. G.; Dai, G. P.; Huang, B. B. *J. Phys. Chem. C* **2009**, *113*, 16394−16401.
(18) Zhang, Y. H.; Tang, Z. R.; Fu, X. Z.; Xu, Y. J. *Appl. Catal., B* **2011**, *106*, 445−452.
(19) Elahifard, M. R.; Rahimnejad, S.; Haghighi, S.; Gholami, M. R. *J. Am. Chem. Soc.* **2007**, *129*, 9552−9553.
(20) Cao, J.; Luo, B. D.; Lin, H. L.; Chen, S. F. *J. Hazard. Mater.* **2011**, *190*, 700−706.
(21) Xu, D. Y.; Lu, P.; Dai, P.; Wang, H. Z.; Ji, S. F. *J. Phys. Chem. C* **2012**, *116*, 3405−3413.
(22) Liu, B.; Zeng, H. C. *Chem. Mater.* **2008**, *20*, 2711−2718.
(23) Bouazza, N.; Ouzzine, M.; Lillo-Ródenas, M. A.; Eder, D.; Linares-Solano, A. *Appl. Catal. B* **2009**, *92*, 377−383.
(24) Xu, Y. J.; Zhuang, Y. B.; Fu, X. Z. *J. Phys. Chem. C* **2010**, *114*, 2669−2676.
(25) Wang, S.; Gong, Q. M.; Zhu, Y. F.; Liang, J. *Appl. Surf. Sci.* **2009**, *255*, 8063−8066.
(26) An, T. C.; Chen, J. Y.; Nie, X.; Li, G. Y.; Zhang, H. M.; Liu, X. L.; Zhao, H. J. *ACS Appl. Mater. Interfaces* **2012**, *4*, 5988−5996.
(27) Xin, F.; Li, L. *Composites, Part A* **2011**, *42*, 961−967.

(28) Alimohammadi, F.; Gashti, M. P.; Shamei, A.; Kiumarsi, A. *Superlattices Microstruct.* **2012**, *52*, 50−62.
(29) An, T. C.; Liu, J. K.; Li, G. Y.; Zhang, S. Q.; Zhao, H. J.; Zeng, X. Y.; Sheng, G. Y.; Fu, J. M. *Appl. Catal. A* **2008**, *350*, 237−243.
(30) Wang, S. H.; Zhou, S. Q. *J. Hazard. Mater.* **2011**, *185*, 77−85.
(31) Wang, P.; Huang, B. B.; Qin, X. Y.; Zhang, X. Y.; Dai, Y.; Whangbo, M. H. *Inorg. Chem.* **2009**, *48*, 10697−10702.
(32) Wang, P.; Huang, B. B.; Qin, X. Y.; Zhang, X. Y.; Dai, Y.; Wei, J. Y.; Whangbo, M. H. *Angew. Chem., Int. Ed.* **2008**, *47*, 7931−7933.
(33) An, C. H.; Peng, S.; Sun, Y. G. *Adv. Mater.* **2010**, *22*, 2570−2574.
(34) Wang, D. S.; Xiao, L. B.; Luo, Q. Z.; Li, X. Y.; An, J.; Duan, Y. D. *J. Hazard. Mater.* **2011**, *192*, 150−159.
(35) Nanba, T.; Masukawa, S.; Uchisawa, J.; Obuchi, A. *J. Catal.* **2008**, *259*, 250−259.
(36) Zhang, L.; He, H. *J. Catal.* **2009**, *268*, 18−25.
(37) Dai, W. L.; Cao, Y.; Ren, L. P.; Yang, X. L.; Xu, J. H.; Li, H. X.; He, H. Y.; Fan, K. N. *J. Catal.* **2004**, *228*, 80−91.
(38) Shi, Z. J.; Lian, Y. F.; Liao, F. H.; Zhou, X. H.; Gu, Z. N.; Zhang, Y. G.; Iijima, S. *Solid State Commun.* **1999**, *112*, 35−37.
(39) Liu, J. K.; An, T. C.; Li, G. Y.; Bao, N. Z.; Sheng, G. Y.; Fu, J. M. *Microporous Mesoporous Mater.* **2009**, *124*, 197−203.
(40) Grabowska, E.; Sobczak, J. W.; Gazda, M.; Zaleska, A. *Appl. Catal. B* **2012**, *117*−*118*, 351−359.
(41) Chen, C. Y.; Jafvert, C. T. *Environ. Sci. Technol.* **2010**, *44*, 6674−6679.
(42) Kong, L.; Jiang, Z.; Lai, H. H.; Nicholls, R. J.; Xiao, T.; Jones, M. O.; Edwards, P. P. *J. Catal.* **2012**, *293*, 116−125.
(43) Kudo, A.; Miseki, Y. *Chem. Soc. Rev.* **2009**, *38*, 253−278.
(44) Wu, T. S.; Wang, K. X.; Li, G. D.; Sun, S. Y.; Sun, J.; Chen, J. S. *ACS Appl. Mater. Interfaces* **2010**, *2*, 544−550.
(45) Zhu, M. S.; Chen, P. L.; Liu, M. H. *Langmuir* **2012**, *28*, 3385−3390.
(46) Torimoto, T.; Ito, S.; Kuwabata, S.; Yoneyama, H. *Environ. Sci. Technol.* **1996**, *30*, 1275−1281.
(47) Yang, D. J.; Liu, H. W.; Zheng, Z. F.; Yuan, Y.; Zhao, J. C..; Waclawik, E. R.; Ke, X. B.; Zhu, H. Y. *J. Am. Chem. Soc.* **2009**, *131*, 17885−17893.
(48) Chen, C. C.; Ma, W. H.; Zhao, J. C. *Chem. Soc. Rev.* **2010**, *39*, 4206−4219.